Available online at www.sciencedirect.com
ScienceDirect
Ceramics International 37 (2011) 3101–3108
CERAMICS INTERNATIONAL
www.elsevier.com/locate/ceramint

Solution combustion synthesis and physicochemical characterization of ZrO_2–MoO_3 nanocomposite oxides prepared using different fuels

Satish Samantaray [a], B.G. Mishra [a,*], D.K. Pradhan [b], G. Hota [a]

[a] Department of Chemistry, National Institute of Technology, Rourkela, Orissa, India
[b] Department of Physics, National Institute of Technology, Rourkela, Orissa, India

Received 11 February 2011; received in revised form 12 May 2011; accepted 12 May 2011
Available online 18 May 2011

Abstract

A series of MoO_3–ZrO_2 nanocomposite oxides with MoO_3 content in the range of 2–20 mol% were prepared by solution combustion method. Three different fuels namely urea, glycine and hexamethylenetetramine (HMTA) were used for the preparation of MoO_3–ZrO_2 oxides. For the sake of comparison, the MoO_3–ZrO_2 composite oxides were also prepared by impregnation of zirconia with molybdenum salt precursor and subsequent heat treatment. The synthesized nanomaterials were characterized by XRD, SEM, TEM and UV–vis spectroscopic technique. XRD study indicated selective stabilization of the tetragonal phase of zirconia in the presence of MoO_3. The method of preparation was found to be crucial for the phase composition of zirconia in the composite oxide. The crystallite size and rms stain were calculated from the Fourier line shape analysis of the broadened X-ray diffraction profiles. With increase in the MoO_3 content, the crystallite size of the tetragonal zirconia phase was found to be decreased. TEM study indicated the presence of small nanoparticles with size in the 5–10 nm range. UV–vis study of the composite oxide materials revealed well dispersion of the molybdenum oxide component in the form of monomer, dimers and nanoclusters in the zirconia matrix. The nature of fuel was found to be crucial in determining the morphology and shape of the particles.

Keywords: Combustion synthesis; MoO_3–ZrO_2; TEM; Hexamethylene tetraamine; Fourier analysis

1. Introduction

Combustion synthesis is an attractive method for preparation of homogeneous, finely dispersed crystalline uni- and multi-component oxides [1–6] as well as metals and alloys of uniform composition and size [7,8]. The specific advantages of combustion synthesis method over other methods of material preparation are (1) single step process, (2) less time consuming, (3) formation of metastable phases and (4) formation of homogeneous nanoparticles [1,2,5]. Several classes of materials with diverse properties such as oxides, nitrides, carbides, complex oxides, metals and alloys have been prepared by combustion synthesis for a variety of technological applications [1–8]. In past few years, many novel procedures have been adopted during combustion synthesis such as use of organic compounds as fuels, microwave and sonic wave as energy source to obtain materials with desired properties. The solution combustion method, one of the convenient modifications of self-propagating high temperature synthesis is widely used for material preparation [2]. In solution combustion method, organic compounds containing reducible functional groups are employed as fuels and metal nitrates are used as oxidizers. The exothermic combustion reaction between the fuel and the oxidizer results in the formation of unagglomerated solid particles with simultaneous evolution of large amounts gaseous products [3–6]. The nature and amount of fuel in a combustion mixture can effectively control the particle size and morphology of the final products. In certain cases, the phase transformation and formation of metastable phases are facilitated by the amount and nature of the fuel. For example, the metastable phase formation of zirconia [9,10] and titania [11] are affected by the amount of fuel. The fuel content in the combustion mixture can also affect the oxidation state of the metal ions in the final oxide. Ranga Rao et al. have reported the formation of CuO, Cu_2O and Cu phases at different fuel content using carbohydrazide as fuel [7]. It is believed that the fuel

* Corresponding author. Tel.: +91 661 2462651; fax: +91 661 2462651.
E-mail address: brajam@nitrkl.ac.in (B.G. Mishra).

0272-8842/$36.00
doi:10.1016/j.ceramint.2011.05.047

binds with the metal cation forming coordination compounds which are soluble in water [1,2]. Nitrogen containing compounds are widely employed as fuel because of their natural tendency to act as chelating ligands forming complexes with the metal ions. Compounds containing N–N bonds in their moieties are particularly useful as fuel for the combustion process [12]. Patil et al. have outlined some important criteria for selection of fuel which include (1) water solubility (2) low ignition temperature (<500 °C) (3) compatibility with metal nitrates, i.e., the combustion reaction should be controlled and smooth and should not lead to explosion and (4) yield no other residual mass except the oxide in question [2,12]. In the present work, we have prepared MoO_3–ZrO_2 composite oxides by the solution combustion method using different fuels and compared their physiochemical characteristics. The potential fuels employed in the present study are urea, glycine and hexamethylene tetraamine, which are fairly common among many organics used in solution combustion synthesis.

$$\frac{F}{O} = -\frac{\sum(\text{Coefficient of elements in the molecular formula of fuel}) \times (\text{valency})}{\sum(\text{Coefficient of elements in the molecular formula of oxidizer salt}) \times (\text{valency})}$$

Molybdenum oxide is a promising material used in many advanced applications such as heterogeneous catalysis [13,14], gas sensing [15], anode material in organic solar cells [16] and electrochromic devices [17]. A variety of MoO_3 based composite oxides such as MoO_3–ZrO_2 [13,14], MoO_3–SiO_2 [14], MoO_3–TiO_2 [15], MoO_3–WO_3 [17] has been reported in literature. These composite oxides show superior physicochemical characteristics and application potential compared to the individual oxide components. The flexibility of the MoO_3 to form different molecular structure and the ability of Mo atoms to assume various oxidation states depending on the processing atmosphere and conditions are the main features that are invoked to explain the properties of these composite oxides [13–17]. Among the different MoO_3 based composite oxide, the ZrO_2–MoO_3 composite oxides are the most extensively investigated system. This stems from the fact that zirconia possess all the required characteristics of a carrier such as high thermal stability, extreme hardness, stability under reducing conditions, and both surface acidic and basic functions. It has been observed that the physicochemical characteristics of the MoO_3–ZrO_2 material depend on the preparation method, the amount of MoO_3 loading and the calcination temperature.

2. Experimental

2.1. Solution combustion synthesis of MoO_3–ZrO_2 composite oxides

Zirconyl nitrate ($ZrO(NO_3)_2{\cdot}xH_2O$), glycine and hexamethylene tetramine (HMTA) were procured from Merck India. Ammonium heptamolybdate and urea were obtained from S.D. fine chemicals ltd., India. All the chemicals were used as received without any further purification. Pure ZrO_2 and MoO_3–ZrO_2 composite oxide materials were prepared by solution combustion synthesis using $ZrO(NO_3)_2{\cdot}xH_2O$, ammonium heptamolybdate as salt precursor and urea, glycine and hexamethylene tetraamine as fuels. In a typical preparation procedure, required amounts of zirconyl nitrate, ammonium heptamolybdate and urea were dissolved in minimum amount of water and the mixture was kept in a furnace, preheated to 400 °C. The mixture instantaneously gets ignited producing a foamy material of MO_3–ZrO_2 simultaneously releasing a lot of gaseous products. The fuel to oxidizer equivalence ratio (F/O) was calculated by summing the total oxidizing and reducing valencies in the fuel and dividing it by the sum of the total oxidizing and reducing valencies in the oxidizer salt [12,18].

The valency of the elements have been assigned by assuming the oxidation state of the elements C, H, O, N, Zr and Mo to be +4, +1, −2, 0, +4 and +6 respectively, in the final product [18]. The F/O ratio was varied from 0.5 to 1.5 to study the effect of fuel content on the physicochemical characteristics of the MoO_3–ZrO_2 composite oxide materials. Using this procedure, MoO_3–ZrO_2 oxides with MoO_3 content of 2, 5, 8, 10, 20 mol% were prepared using urea as fuel. The MoO_3–ZrO_2 materials are referred to as *x*MoZr-Y in the text, where x represents the mol% of MoO_3 present in the composite oxide and Y stands for the fuel employed for the preparation of these composite oxides (Glycine (G), Urea (U) and Hexamethylene tetraamine (H)).

2.2. Synthesis of MoO_3–ZrO_2 composite oxides by impregnation method

For the sake of comparison, the MoO_3 (10 mol%)–ZrO_2 material was also prepared by conventional impregnation method. Pure ZrO_2 was initially prepared by precipitation from $ZrOCl_2{\cdot}8H_2O$ solution using liquid ammonia as precipitating agent at pH 9.0. The hydroxide precursor obtained was washed multiple times with hot water, dried in a hot air oven for 12 h and then calcined in air at 500 °C for 2 h. The impregnation process was carried out by adding the required amount of ammonium heptamolybdate to ZrO_2 aqueous suspension and then stirring for 6 h. The aqueous suspension was then heated with constant stirring to remove water. The resulting material was dried at 120 °C for 12 h followed by calcination at 500 °C for 2 h to obtain the final material. The ZrO_2, MoO_3 (10 mol%)–ZrO_2 materials prepared by this method are referred to as ZrO_2-C and 10MoZr-C.

2.3. Characterization techniques

The XRD patterns of the *x*MoZr-Y and *x*MoZr-C samples were obtained using a Philips PAN analytical diffractometer

using Ni filtered CuKα_1 (λ = 1.5405 Å) radiation in the range of 20–70° at a scan rate of 2°/min. The percentage tetragonal phase present in the composite oxide sample was estimated using the formula reported in literature [13].

$$\%Tetragonal = \frac{IT(2\theta = 30.2)}{IT(2\theta = 30.2 + \left(\frac{IM(2\theta=28.2)+IM(2\theta=31.4)}{2}\right)} \times 100$$

where IT and IM stands for the integral intensity of the XRD peaks at the specified 2θ values for the tetragonal and monoclinic phases, respectively. The crystallite size and rms strain have been calculated from the Fourier line shape analysis following the Warren and Averbach method [19]. The UV–vis absorbance spectra of the samples were recorded using Shimadzu spectrometer model 2450 with $BaSO_4$ coated integration sphere. Scanning electron micrograph (SEM) was taken using JEOL JSM-5300 microscope (acceleration voltage 20 kV). The sample powders were deposited on a carbon tape before mounting on a sample holder. Transmission electron micrographs (TEM) of the samples were recorded using PHILIPS CM 200 equipment using carbon coated copper grids.

3. Results and discussion

3.1. XRD study

The X-ray diffraction patterns of the pure ZrO_2 and 10MoZr materials prepared by combustion as well as conventional impregnation method are presented in Fig. 1. Pure Zirconia prepared by the precipitation method show well defined and intense peaks with *d* values of 3.16, 2.95. 2.85, 2.56, 1.81 and 1.53 Å. These peaks correspond to the presence of both monoclinic and tetragonal phase of zirconia [9,10]. The percentage of tetragonal phase present in the sample is calculated to be 58%. The pure ZrO_2 prepared using different fuels by the combustion method exhibit peaks with *d* values 2.95, 2.58, 1.80 and 1.54 Å corresponding to the presence of tetragonal phase only. The characteristic reflections at 3.16 and 2.85 Å of monoclinic zirconia are not observed for the combustion synthesized zirconia samples. This observation clearly suggests the selective stabilization of the metastable tetragonal phase of zirconia in combustion synthesis process. Among all ZrO_2 synthesized, the ZrO_2-G sample shows considerable broadening of the peaks and low intensity as compared to the ZrO_2-H and ZrO_2-U sample. Addition of MoO_3 onto ZrO_2 matrix has been found to significantly

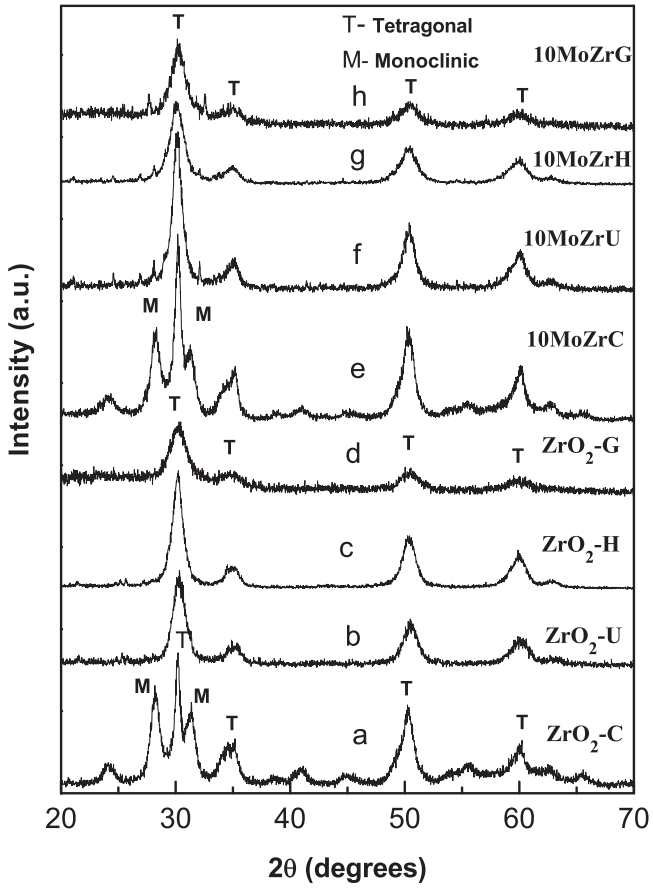

Fig. 1. X-ray diffraction patterns of (a) ZrO_2-C, (b) ZrO_2-U, (c) ZrO_2-H, (d) ZrO_2-G, (e) 10MoZr-C, (f) 10MoZr-U, (g) 10MoZr-H and (h) 10MoZr-G (T and M refers to tetragonal and monoclinic phases of zirconia, respectively).

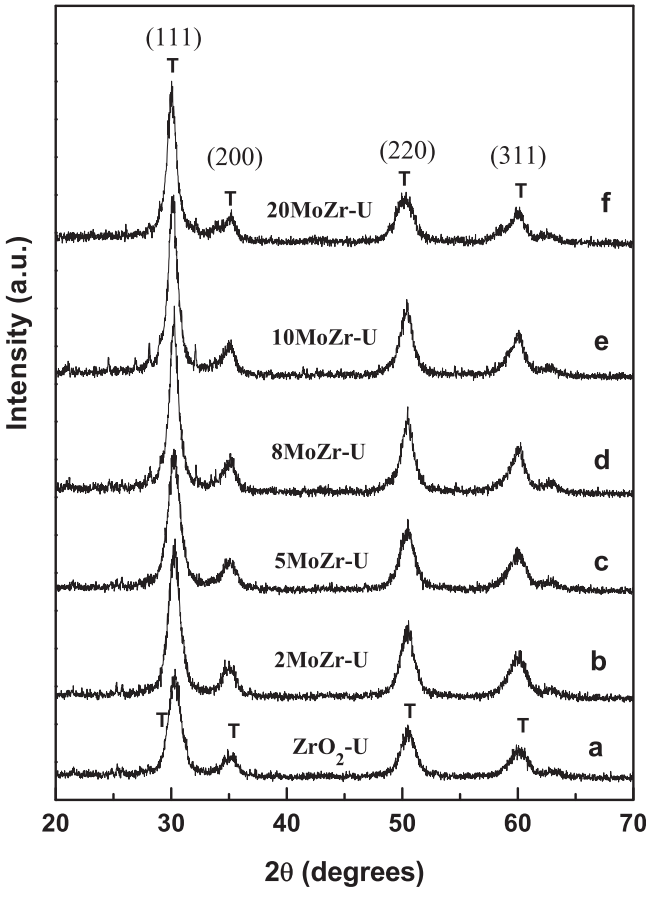

Fig. 2. X-ray diffraction patterns of (a) ZrO_2-U, (b) 2MoZr-U (c) 5MoZr-U, (d) 8MoZr-U (e) 10MoZr-U and (f) 20MoZr-U (All compositions prepared using urea as a fuel, T refers to tetragonal phase).

influence the phase composition of the composite oxide. The 10MoZr-C material prepared by impregnation method found to contain 83% tetragonal phase. All the 10MoZr materials prepared by combustion method show XRD peaks characteristics of tetragonal phase. The XRD patterns of *x*MoZr materials with MoO_3 content in the range of 2–20 wt%, prepared using urea as fuel is presented in Fig. 2. All the materials synthesized show the characteristic reflections corresponding to the tetragonal phase. No separate crystalline phase corresponding to either MoO_3 or $Zr(MoO_4)_2$ was observed in the XRD study. This result suggests the fact that the MoO_3 species are well dispersed in zirconia matrix. In order to study the effect of fuel content in the combustion mixture on the crystallinity and phase transformation behavior of the composite oxides, the 10MoZr material has been prepared at different F/O ratio using glycine and HMTA as fuels. The XRD patterns of the synthesized 10MoZr materials are presented in Fig. 3. The major phase observed in case of both the fuels is tetragonal zirconia. The XRD peak intensity has been found to increase with fuel content. The increase in exothermicity of the combustion reaction with fuel content can lead to well crystalline materials which show well defined intense peaks. In case of HMTA fuel two low intense peaks are observed at 2θ values of 27.5° and 32.5°. These peaks correspond to the presence of a small amount of $Zr(MoO_4)_2$ spinel phase (JCPDS file No. 39-1438). No separate crystalline phase corresponding to the presence of MoO_3 is observed in the XRD patterns of the composite oxide. The crystallite size and rms stain are calculated from the Fourier line shape analysis for all the combustion synthesized samples following the Warren and Averbach method [19] using software BRAEDTH and the details are available in literature [20]. The peak position (2θ), full width at half maximum (FWHM) and intensity are calculated using commercially available software (PEAK FIT) for each peak of the XRD data. The indexing of all peaks of XRD patterns are carried out using 2θ and intensity value of each peak by a standard computer software POWD [21]. The best agreement between the observed and the calculated interplaner spacing and Bragg angles is found for tetragonal crystal structure. The calculated volume-weighted distributions, (pV), and crystallite size as function of the Fourier length (L) for the different zirconia samples is given in Fig. 4(a) and (b) respectively. The wide distribution function observed for the ZrO_2-H sample indicates that the particles are polycrystalline with larger particle size. The ZrO_2-G material shows a narrower size distribution function as compared to the ZrO_2-U and ZrO_2-H materials (Fig. 4a). The crystallite sizes of the ZrO_2-G, ZrO_2-U and ZrO_2-H materials are found to be 9, 30 and 49 nm

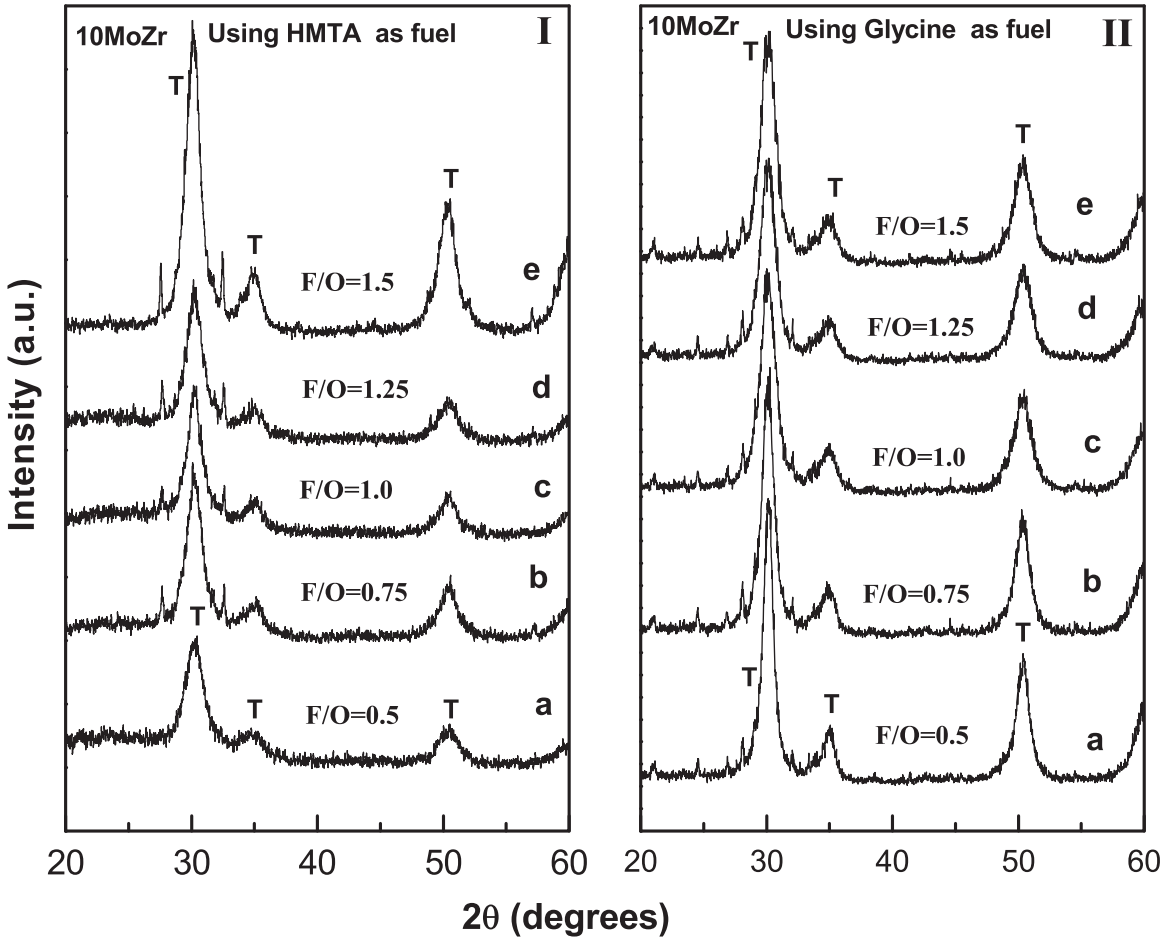

Fig. 3. X-ray diffraction patterns of 10MoZr catalyst prepared using hexamethylene tetraamine as fuel (Panel I) and glycine as fuel (Panel II) at different fuel to oxidizer ratio in the range of F/O = 0.5–1.5 (T refers to the tetragonal phase).

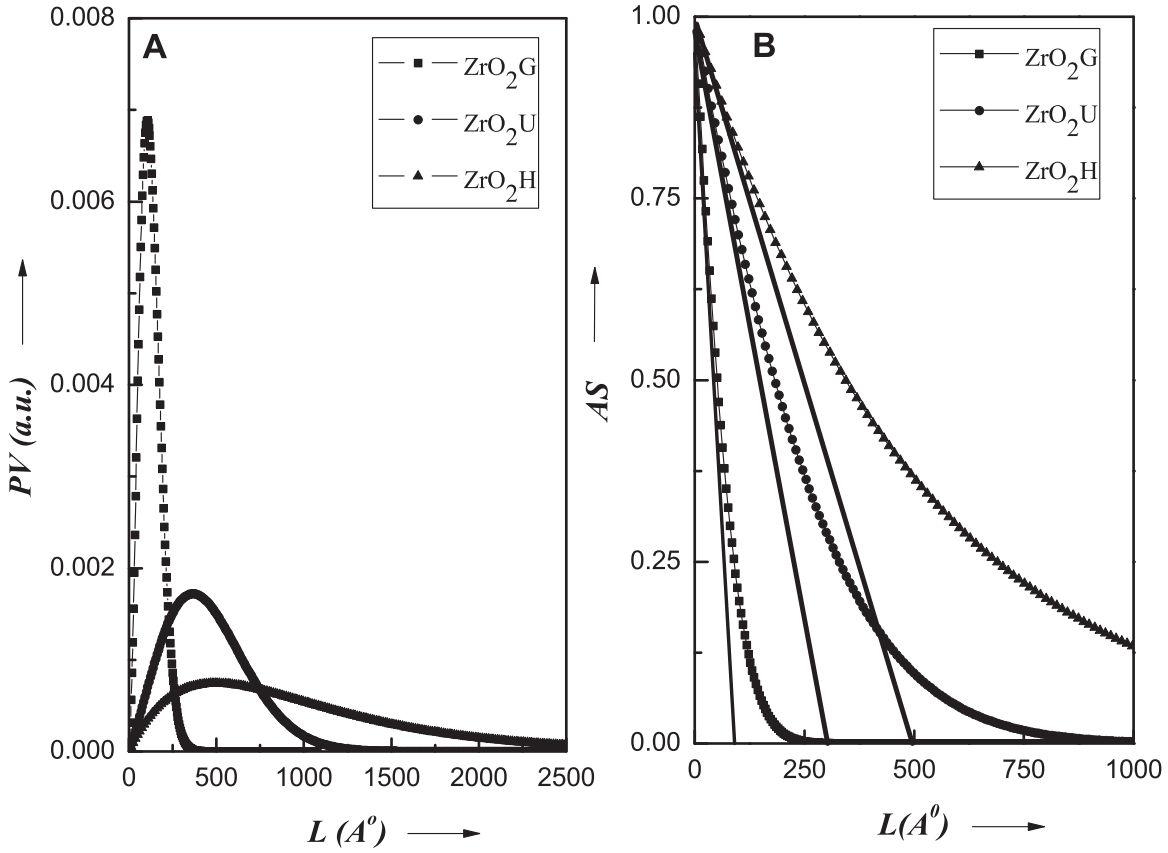

Fig. 4. Fourier line profile analysis plots for the ZrO_2-U, ZrO_2-H and ZrO_2-G materials.

respectively (Fig. 4b). The least-squares refined lattice parameters, the unit cell volume, crystallite size and rms strain of *x*MoZr-U materials with different percentage of MoO_3 is presented in Table 1. With increase in Mo concentration there is a decrease in the crystallite size and increase in the strain observed for the nanocomposite oxide. The increase in the rms strain may be due to the higher disorder corresponding to the random and local lattice distortion. The Fourier line shape analysis data for the 10MoZr-G materials prepared at different F/O ratio along with the pure ZrO_2-G material is shown in Table 2. For different F/O ratio, first there is decrease in the crystallite size up to F/O ratio 0.75, after that the crystallite size is found to be increased. The increase in the crystallite size at higher F/O ratio is due to the increase in exothermicity of the combustion reaction [10]. It has been reported that the adiabatic reaction temperature (T_d) increases with fuel content in the combustion mixture [10,22]. In the present study, it is believed that the higher adiabatic temperature at F/O = 1.5 is responsible for the possible agglomeration of the nanoparticles giving larger particle size. The reverse trend is observed for the rms strain. The crystallite size calculations are also carried out for 10MoZr-H materials prepared at different F/O ratio and found to be in the range of 10–50 nm.

3.2. UV–vis study

The UV–vis spectra of the combustion synthesized *x*MoZr materials are presented in Fig. 5. Pure Zirconia is a direct band gap insulator which shows interband transition in the UV region of the electronic spectrum corresponding to the $O^{2-}(2p) \rightarrow Zr^{4+}$ (4d) charge transfer transition. Among the polymorphic forms of

Table 1
The lattice parameters, unit cell volume, crystallite size and rms strain of *x*MoZr-U materials.

Fuel	Materials	*a* in Å	*c* in Å	Volume (Å^3)	Size (nm)	Strain $\langle e^2 \rangle^{1/2}$
Urea	ZrO_2	5.1505	5.1844	137.53	30	3.84×10^{-3}
	2MoZr	5.1555	5.1796	137.67	37	3.34×10^{-3}
	5MoZr	5.1568	5.1785	137.71	28	3.98×10^{-3}
	8MoZr	5.1542	5.1808	137.63	8	7.43×10^{-3}
	10MoZr	5.1361	5.1820	136.70	6	7.97×10^{-3}
	20MoZr	5.1338	5.1796	136.51	5	1.26×10^{-2}

Table 2
The lattice parameters, unit cell volume, crystallite size and rms strain of ZrO_2-G and 10MoZr-G materials.

Fuel	Materials	*a* in Å	*c* in Å	Volume (Å^3)	Size (nm)	Strain $\langle e^2 \rangle^{1/2}$
Glycine	ZrO_2	5.1543	5.1809	137.64	9	6.51×10^{-3}
10MoZr-G	F/O = 0.5	5.1568	5.1785	137.71	7	5.81×10^{-3}
	F/O = 0.75	5.1644	5.1714	137.93	4	1.26×10^{-2}
	F/O = 1.0	5.1531	5.1821	137.61	11	7.21×10^{-3}
	F/O = 1.25	5.1361	5.1820	136.70	15	5.66×10^{-3}
	F/O = 1.5	5.1518	5.1833	137.57	39	3.88×10^{-3}

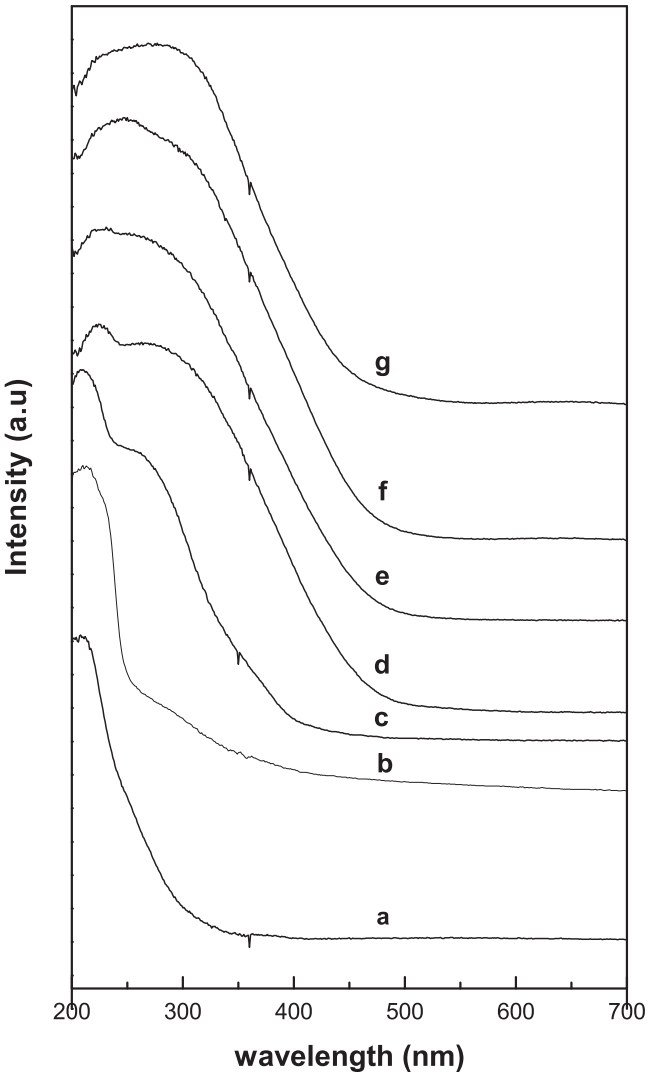

Fig. 5. UV–vis spectra of MoZr catalyst (a) ZrO_2-U, (b) ZrO_2-H, (c) ZrO_2-G, (d) 2MoZr-U, (e) 5MoZr-U, (f) 10MoZr-U and (g) 20MoZr-U.

zirconia, the octacoordinated tetragonal (space group F*m*3*m*) and cubic (space group $P4_2/nmc$) phases show UV absorption maxima in the range of 200–210 nm where as the heptacoordinated monoclinic phase (space group $P2_1/c$) shows maxima around 240 nm [23]. It has been observed that as the coordination number of Zr^{4+} ion decreases from 8 to 6, the LMCT absorption maxima progressively shifts to lower energy (higher wavelength) [24,25]. The combustion synthesized ZrO_2 prepared using glycine and HMTA as fuel show only one absorption band at 210 nm whereas ZrO_2 prepared using urea as fuel shows absorption band at 210 nm in addition to a broad shoulder at ∼280 nm. The prominent absorption band observed at peak maxima of 210 nm has been assigned to the $O^{2-} \rightarrow Zr^{4+}$ Charge transfer transition arising out of the tetragonal polymorph of zirconia. This observation is complementary to the XRD result where selective stabilization of tetragonal phase has been observed for the combustion synthesized samples. The broad band observed at 280 nm for ZrO_2-U sample can be ascribed to the transition arising out of structural imperfaction and defect centre present in the nanosize crystallite of zirconia. The presence of structural disorder and defect centres shift the adsorption edge to higher wavelength due to the presence of localized states between the valence and conduction band. It is likely that the zirconia particles synthesized by combustion method using urea as fuel can contain defect sites which contribute to the broad absorption feature in the higher wavelength side of the spectrum. Pure MoO_3 shows two well defined absorption bands at 240 and 320 nm (plot not shown). Since Mo^{6+} has a d^0 electronic configuration, the only absorption feature expected is due to the ligand–metal charge transfer transition (LMCT), $O^{2-} \rightarrow Mo^{6+}$ which occur in the range of 200–400 nm. However, depending on the coordination preference and local symmetry of the Mo (VI) ions different absorption bands are observed in the electronic spectrum. The peak at 240 nm for pure MoO_3 can be assigned to the isolated MoO_4 species with tetrahedral symmetry where as the peak at 320 nm can be assigned to bulk polymolybdate species present in the sample [26–28]. The addition of MoO_3 to zirconia matrix significantly modifies the absorption spectra of the combustion synthesized MoO_3–ZrO_2 composite oxide. For samples with low MoO_3 loading (2 and 5 wt%) a prominent band is observed at 226 nm along with a broad shoulder at 280 nm. The sharp and narrow absorption band at 226 nm can be assigned to the tetrahedrally coordinated isolated molybdate species with structural distortion. Henker et al. in their study of supported molybdate species has compared the absorption spectra of Na_2MoO_4 and $Na_2MoO_4{\cdot}2H_2O$ [26]. It has been observed that the Na_2MoO_4 with tetrahedral Mo ions shows absorption peak at 245 nm where as in $Na_2MoO_4{\cdot}2H_2O$ where the tetrahedral Mo is distorted due to the water of crystallization shows band maxima at 225 nm. In the present study, the assignment of the peak at 226 nm to structurally distorted tetrahedral isolated molybdate species is in accordance with the observation by Henker et al. [26]. The broad peak at 280 nm can be assigned to small nanosize molybdate clusters dispersed on the surface of the zirconia. Liu et al. have studied supported MoO_3 system using UV–vis spectroscopy and assigned the peak at ∼300 nm to the presence of heptamolybdate clusters [28]. In the present case it is likely that such clusters can exist on the surface of zirconia in a well dispersed state. When the percentage MoO_3 loading is increased to 10 percent and higher, two broad absorption features with maxima at 250 nm and >300 nm are observed. Earlier studies on the UV–vis spectra of MoO_3 system have revealed three absorption regions corresponding to the presence of isolated molybdate species (220–250 nm), polymolybdate clusters (260–290 nm) and bulk type molybdate (>315 nm) [26–28]. The peak observed at 250 nm for sample with higher loading thus can be assigned due to the polymolybdate clusters. Whereas the broad peak peak with maxima >300 nm can be assigned to the presence of bulk type molybdate species present on the surface of zirconia. However it is likely that the bulk type MoO_3 can exist in amorphous form which has escaped XRD detection. The UV–vis study of the combustion synthesized MoZr sample implies the presence of well dispersed molybdate species in the form of isolated and polymolybdate clusters on the surface of zirconia.

3.3. SEM and TEM study

The scanning electron micrographs of ZrO_2-U, ZrO_2-H and ZrO_2-G are presented in Fig. 6. The nature of the fuel is found to have a profound influence on the morphology of synthesized zirconia particles. The choice of fuel is critical in deciding the exothermicity of the redox reaction between the metal nitrate and the fuel. The zirconia particles synthesized using urea as fuel is found to be of low density and spongy in nature (Fig. 6a). Similar observation is noted for HMTA fuel with numerous elongated macropores present on the surface of the particle (Fig. 6b). Zirconia nanoparticles prepared using glycine as fuel are dense and with well defined shape (Fig. 6c). The spongy nature of zirconia particles in case of urea can be ascribed to the evolution of large amount of gases during combustion. Theoretically, for the formation of one mole of zirconia, 8.66, 7.5 and 5.8 mol of gases are generated using urea, glycine and HMTA as fuel respectively. The higher amount of gases generated leaves the material porous and spongy. The difference in morphology may be related to the inherent nature of the fuel, their binding characteristics and amount of gases evolved during their decomposition [2,10,16]. Urea and glycine can act as bidentate ligand and can coordinate to the metal ions in the combustion mixture. However, urea is basic where as glycine is amphoteric in nature which can have different degree of bonding with the metal ions. HMTA on the other hand is a tetradentate ligand which is known to release ammonia in aqueous solution. Zirconium ions being acidic in nature can undergo considerable hydrolysis in the presence of urea and HMTA. The uncontrolled hydrolysis of the Zr^{4+} ions and subsequent combustion can lead to particles with random morphology and sizes. The zwiterionic character of glycine molecule on the other hand is useful in effectively complexing with metal ions of varying ionic sizes. This in turn helps in preventing their selective precipitation and maintains a compositional homogeneity among the constituents [22]. Hence the uniform morphology of the combustion synthesized

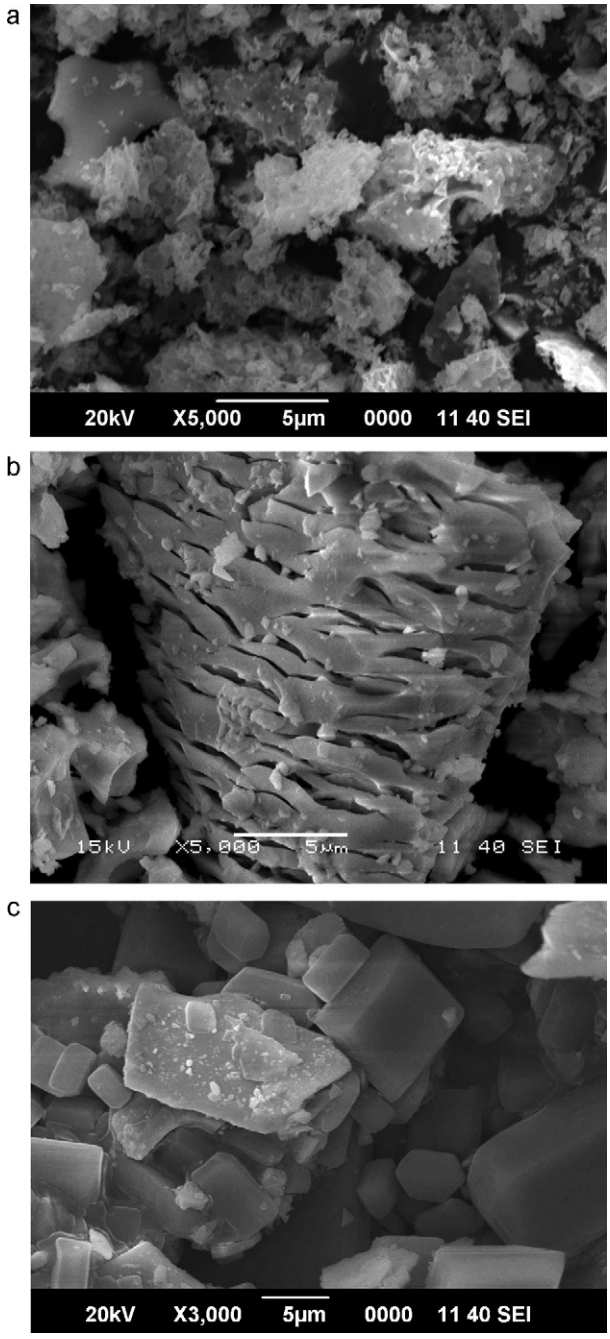

Fig. 6. Scanning electron micrograph of (a) ZrO_2-U, (b) ZrO_2-H, and (c) ZrO_2-G.

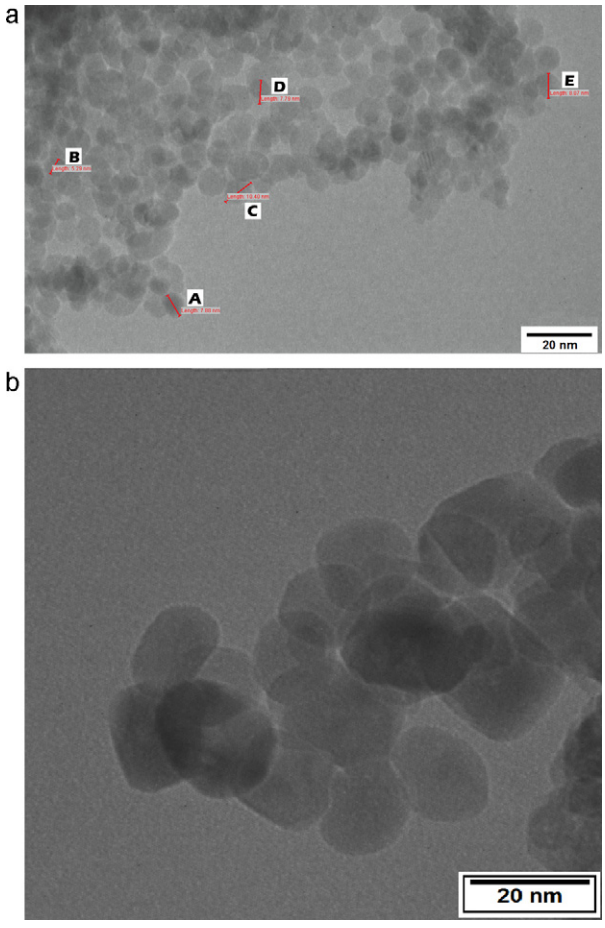

Fig. 7. Transmission electron micrograph of (a) ZrO_2-G and (b) 10MoZr-G material (particle size of the marked particles A, B, C, D and E in the TEM image (a) are 7.9, 5.3, 10.4, 7.8 and 8.1 nm, respectively).

particles can be ascribed to the effective complexation and prevention of hydrolysis of the ions in the combustion mixture. The transmission electron micrograph of the ZrO_2-G and 10MoZr-G material is shown in Fig. 7. Uniform zirconia nanoparticles with size in the range of 5–10 nm are observed in the TEM picture (Fig. 7a). The 10MoZr-G material synthesized using glucine as fuel at the stoichiometric F/O ratio shows particles with size in the range of 10–15 nm (Fig. 7b). The Fourier line shape analysis data is found to be complimentary to the TEM observation. The TEM observations indicate that combustion synthesis is quite effective for preparation of nanocomposites. During combustion synthesis process, the reactants are uniformly dispersed at molecular level in the combustion mixture. When combustion occurs, the nucleation and growth of the particles take place only through the short-distance diffusion of the nearby atoms. Due to the shorter life span of the combustion reaction, the long-distance diffusion of the atoms is not facilitated resulting in the formation of nanosized materials.

4. Conclusion

In this investigation, we have prepared a series of MoO_3–ZrO_2 nanocomposite oxides by combustion synthesis process and characterized by XRD, UV–vis-DRS, TEM and SEM techniques. The composite oxides contain predominantly tetragonal phase of zirconia. No separate crystalline phase corresponding to the bulk MoO_3 is observed in the composition range of 2–20 mol% of MoO_3, which indicate well dispersion of the molybdenum oxide in the zirconia matrix. Fourier line shape analysis of the XRD profiles indicate that the crystallite sizes are in the range of 4–40 nm depending upon the fuel employed. With decrease in size the rms strain has been found to increase. Glycine as fuel is quite effective in producing nanoparticles with uniform morphology and smaller size. TEM studies of the combustion synthesized samples indicate the presence of 5–15 nm size particles. The inherent nature of the fuel and its complexing capability with the ionic species is crucial for the production of particle with uniform shape and morphology. UV–vis study of the composite oxide revealed the presence of well dispersed MoO_3 species in the form of monomer, dimers and nanoclusters in the zirconia matrix.

Acknowledgement

The authors would like to thank Council of Scientific and Industrial Research, New Delhi for financial support.

References

[1] C.N.R. Rao, Chemical Approaches to the Synthesis of Inorganic Materials, Wiley Eastern Limited, New Delhi, 1994.
[2] K.C. Patil, S.T. Aruna, T. Mimani, Combustion synthesis: an update, Curr. Opin. Solid State Mater. Sci. 6 (2002) 507–512.
[3] M.A. Naik, B.G. Mishra, Combustion synthesized WO_3–ZrO_2 nanocomposites as catalyst for the solvent-free synthesis of coumarins, Colloids Surf. A 317 (2008) 234–238.
[4] G. Ranga Rao, H.R. Sahu, B.G. Mishra, Surface and catalytic properties of Cu–Ce–O composite oxides prepared by combustion method, Colloids Surf. A 220 (2003) 261–269.
[5] Z. Yermekova, Z. Mansurov, A. Mukasyan, Influence of precursor morphology on the microstructure of silicon carbide nanopowder produced by combustion syntheses, Ceram. Int. 36 (2010) 2297–2305.
[6] C. Peng, Z. Zhang, Nitrate–citrate combustion synthesis of $Ce_{1-x}Gd_xO_{2-x/2}$ powder and its characterization, Ceram. Int. 33 (2007) 1133–1136.
[7] G. Ranga Rao, B.G. Mishra, H.R. Sahu, Synthesis of CuO, Cu and CuNi alloy particles by solution combustion using carbohydrazide and *N*-tertiarybutoxy-carbonylpiperazine fuels, Mater. Lett. 58 (2004) 3523–3527.
[8] L. Li, I. Saita, K. Saito, T. Akiyama, Hydriding combustion synthesis of hydrogen storage alloys of Mg–Ni–Cu system, Intermetallics 10 (2002) 927–932.
[9] K.R. Venkatachari, D. Haung, S.P. Ostrander, W.A. Schulze, G.C. Stangle, A combustion synthesis process for synthesizing nanocrystalline zirconia powders, J. Mater. Res. 10 (1995) 748–755.
[10] H.R. Sahu, G. RangaRao, Characterization of combustion synthesized zirconia powder by UV–vis, IR and other techniques, Bull. Mater. Sci. 23 (2000) 349–354.
[11] H.-K. Ma, H.-A. Yang, Combustion synthesis of titania nanoparticles in a premixed methane flame, J. Alloys. Compd. 504 (2010) 115–122.
[12] K.C. Patil, M.S. Hegde, T. Rattan, S.T. Aruna, Chemistry of Nanocrystalline Oxide Materials, World Scientific Publishing Co. Pte. Ltd., 2008.
[13] E.A. El-Sharkawy, A.S. Khder, A.I. Ahmed, Structural characterization and catalytic activity of molybdenum oxide supported zirconia catalysts, Micropor. Mesopor. Mater. 102 (2007) 128–137.
[14] S.M. Kemdeo, V.S. Sapkal, G.N. Chaudhari, TiO_2–SiO_2 mixed oxide supported MoO_3 catalyst: physicochemical characterization and activities in nitration of phenol, J. Mol. Catal. A: Chem. 323 (2010) 70–77.
[15] Y.X. Li, K. Galatsis, W. Wlodarski, M. Passacantando, S. Santucci, P. Siciliano, M. Catalano, Microstructural characterization of MoO_3–TiO_2 nanocomposite thin films for gas sensing, Sens. Actuators B: Chem. 77 (2001) 27–34.
[16] L. Cattin, M. Morsli, F. Dahou, S. Yapi Abe, A. Khelil, J.C. Bernède, Investigation of low resistance transparent MoO_3/Ag/MoO_3 multilayer and application as anode in organic solar cells, Thin Solid Films 518 (2010) 4560–4563.
[17] T. Ivanova, K.A. Gesheva, G. Popkirov, M. Ganchev, E. Tzvetkova, Electrochromic properties of atmospheric CVD MoO_3 and MoO_3–WO_3 films and their application in electrochromic devices, Mater. Sci. Eng. B 119 (2005) 232–239.
[18] S.R. Jain, K.C. Adiga, V.R. Verneker, A new approach to thermochemical calculations of condensed fuel-oxidizer mixtures, Combust. Flame 40 (1981) 71–79.
[19] B.E. Warren, B.L. Averbach, The effect of cold-work distortion on X-ray patterns, J. Appl. Phys. 21 (1950) 595–599.
[20] D. Balzar, H. Ledbetter, Voigt-function modeling in fourier analysis of size- and strain-broadened X-ray diffraction peaks, J. Appl. Crystallogr. 26 (1993) 97–103.
[21] "POWD", An interactive powder diffraction data interpretation and indexing programme, ver. 2.1 E. Wu, School of Physical Science, Flinder Univ. of South Australia, BedfordPark, Australia.
[22] J. Kishan, V. Mangam, B.S.B. Reddy, S. Das, K. Das, Aqueous combustion synthesis and characterization of zirconia–alumina nanocomposites, J. Alloys Compd. 490 (2010) 631–636.
[23] E.F. López, V.S. Escribano, M. Panizza, M.M. Carnascialic, G. Busca, Vibrational and electronic spectroscopic properties of zirconia powders, J. Mater. Chem. 11 (2001) 1891–1897.
[24] M. Scheithauer, R.K. Grasselli, H. Knozinger, Genesis and structure of WO_x/ZrO_2 solid acid catalysts, Langmuir 14 (1998) 3019–3029.
[25] M. Li, Z. Feng, G. Xiong, P. Ying, Q. Xin, C. Li, Phase transformation in the surface region of zirconia detected by UV Raman spectroscopy, J. Phys. Chem. B 105 (2001) 8107–8111.
[26] M. Henker, K.P. Wendlandt, J. Valyon, Structure of MoO_3/Al_2O_3–SiO_2 catalysts, Appl. Catal. A 69 (1991) 205–220.
[27] M.M. Mohamed, S.M.A. Katib, Structural and catalytic characteristics of MoO_3/CeO_2 catalysts: CO oxidation activity, Appl. Catal. A 287 (2005) 236–243.
[28] Z. Liu, Y. Chen, Spectroscopic studies on tetragonal ZrO_2-supported MoO_3 and NiO–MoO_3 systems, J. Catal. 177 (1998) 314–324.